MIT Open Access Articles

Predicted X-ray backgrounds for the International X-ray Observatory

Massachusetts Institute of Technology

Predicted X-ray Backgrounds for the International X-ray Observatory

R. K. Smith[1], M. W. Bautz[2], J. Bookbinder[1], M. R. Garcia[1], M. Guainazzi[3] C. A. Kilbourne[4],
[1]Smithsonian Astrophysical Observatory, [2]Massachusetts Institute of Technology,
[3]ESA European Space Astronomy Center, [4]NASA Goddard Space Flight Center

ABSTRACT

The background that will be observed by IXO's X-ray detectors naturally separates into two components: (1) a Cosmic X-ray Background (CXB), primarily due to unresolved point sources at high energies (E>2 keV), along with Galactic component(s) at lower energies that are generated in the disk and halo as well as the Local Bubble and charge exchange in the heliosphere, and (2) a Non-X-ray Background (NXB) created by unvetoed particle interactions in the detector itself. These may originate as relativistic particles from the Sun or Galactic Cosmic Rays (GCR), creating background events due to both primary and secondary interactions in the spacecraft itself. Stray light and optical transmission from bright sources may also impact the background, depending upon the design of the baffles and filters.

These two components have distinct effects on observations. The CXB is a sum of power-law, thermal, and charge exchange components that will be focused and vignetted by the IXO mirrors. The NXB, in contrast, is due to particle, not photon, interactions (although there will be some fluorescence features induced by particle interactions), and so will not show the same effects of vignetting or trace the effective area response of the satellite. We present the overall background rates expected from each of these processes and show how they will impact observations. We also list the expected rates for each CXB process using both mirror technologies under consideration and the predicted NXB for each detector.

Keywords: IXO, instrumentation: background, X-rays: diffuse, cosmic rays

1. INTRODUCTION

The International X-ray Observatory (IXO) will measure X-rays from galaxy clusters, supermassive black holes, and X-ray binaries as well as a range of other sources, Galactic and extragalactic. The mission will address questions ranging from the equation of state of neutron stars to the structure and evolution of the Universe. To accomplish these tasks, the IXO design calls for a 3+ m diameter grazing-incidence mirror with a 20m focal length and a 5 arcsec HEW PSF. Two mirror technologies are under consideration, the Silicon Pore Optic (SPO) or Slumped Glass Optic (SGO)[1]. The observatory itself contains five distinct instruments, including the X-ray Microcalorimeter Spectrometer (XMS), a high-spectral-resolution imager, and the Wide Field Imager/Hard X-ray Imager (WFI/HXI), a silicon-based dual detector with a wide field of view and moderate spectral resolution. In addition, the instrument complex includes a non-imaging High Time Resolution Spectrometer (HTRS), an imaging X-ray Polarimeter (XPOL), and a slitless X-ray Grating Spectrometer (XGS). This paper will focus on the first two detectors, which are the primary imagers and the most likely to be impacted by background.

The XMS features a core 40×40 array of 300 μm pixels, embedded within a 52×52 pixel array of 600 μm pixels. The core array thus has a FOV of ~2.1×2.1 arcmin[2], while the full detector FOV is ~5.4×5.4 arcmin[2]. The WFI/HXI is a dual detector, with the WFI in focus and the HXI immediately behind it. The WFI is an Active Pixel Sensor with an array of 1024×1024 100 μm pixels and a circular field of view ~18 arcmin in diameter. The HXI uses 250 um pixels and a 8.25x8.25 arcmin[2] field of view. We will review the sources of background and discuss their impact on these detectors.

2. THE COSMIC X-RAY BACKGROUND

The CXB contains components from 'local' (including both the Solar system and the so-called Local Hot Bubble (LHB)[2]), Galactic, and extragalactic sources. These components generate both a line and continuum background, and all are subject to a certain amount of debate as to their origin and correct spectrum. We discuss each in turn.

2.1 Solar Wind Charge Exchange

Solar Wind Charge Exchange (SWCX) itself arises from the Earth's exosphere and the Solar system's heliosphere[3]. The SWCX component creates low energy (E<1.5 keV) emission lines due to electron cascades following transfers from neutral material either in the Earth's exosphere or the heliosphere onto highly ionized solar wind ions. SWCX emission can be quite strong compared to other backgrounds in the E<1.5 keV bandpass; X-ray observations have even been sug-

gested as a way to measure sudden sharp increases in the solar wind flux and study the Earth's magnetosheath[4]. The exact spectrum of SWCX is unknown (measurement would require an X-ray microcalorimeter), although models exist[5].

As noted by Kuntz & Snowden[6], "The exospheric contribution itself has two sources: direct interaction of the solar wind with the exospheric neutrals and interaction within the magnetosheath where the solar wind density is enhanced and its velocity reduced." Chandra and XMM-Newton have detected the exospheric SWCX component primarily as 'flares' seen in soft X-ray emission during periods of strong solar winds combined with observations in particular viewing geometries[7]. These SWCX flares are not the same as traditional 'solar flares' due to particle ejection from the Sun, as SWCX creates true cosmic (if local) X-rays while the particles in solar flares can only create non-X-ray backgrounds. IXO's orbit at L2 ensures it will see no exospheric neutral component arising from the Earth's atmosphere. The

Figure 1 – Proposed IXO Orbit. Note that the satellite will orbit in and out of the Earth's bow shock, but is always outside the magnetotail.

SWCX created due to interactions with the magnetosheath may be significant[8], even if IXO is outside the magnetotail itself (see Figure 1). The extent of this effect remains uncertain, as one survey[9] of XMM-Newton observations found no clear connection between enhanced SWCX emissions and sightlines near the magnetosheath in the region between the Sun and Earth while another does suggest a link[10].

The heliospheric SWCX component is generated throughout the solar system as solar wind ions find neutral hydrogen or helium atoms. As a result heliospheric SWCX is thought to be a continuous low-level component, although its strength apparently varies with time and look direction[8,9,10,11]. The minimum flux from the heliospheric component is not known, because of the unknown contribution of the Local Hot Bubble. However, the XMM-Newton survey found that the SWCX contribution to the O VII (~0.57 keV) and O VIII (~0.65 keV) surface brightnesses was generally less than 4 ph/ cm^2/s/sr (Line Units, hereafter LU) and less than 2 LU, respectively. The SWCX contribution generates a soft X-ray line spectrum, not a continuum, with many more lines expected at E < 0.4 keV that are not resolved by current detectors. This component of the SWCX is the only cosmic X-ray background component that could change from existing measurements done with Earth-orbiting satellites due to IXO's L2 orbit.

2.2   The Local Hot Bubble

The second component, from the LHB, is usually modeled as a ~10^6 K thermal plasma[12]. Like the SWCX component, X-rays from the LHB are line dominated[13]. Although both components are strongest in the 0.1-0.3 keV band, the best-measured lines are from O VII and O VIII at ~0.57 and 0.65 keV, respectively. O VII emission lines have been observed with a surface brightness of ~1-3 LU[14]. The origin of this line is in dispute; likely, it is created by some combination of SWCX and the LHB. Regardless, at the energy of the O VII lines the result is non-trivial as IXO effective area exceeds 1 m^2; even 1 LU will generate ~10^{-3} counts/s/arcmin^2 per sq. meter of effective area. The overall LHB can be modeled as a thermal plasma with parameters given in Table 2[15].

Galactic Emission

The Galactic component varies dramatically with look direction; obviously the background from the Galactic plane is quite different from the Galactic halo. In particular, observations done at low (l<5°) Galactic latitude will have a background due to various Galactic sources that are only 'background' in the context of a particular observation. However, even at higher latitudes the Galactic halo is known to be 'patchy'[16], with some regions that can be fit with a 3×10^{6}K and others that show little hot emission. This also affects primarily the low (E<1 keV) energy part of the spectrum, and like the SWCX and LHB contributions will create a spectrum that is line rather than continuum dominated.

The overall average Galactic background can be modeled as two thermal plasmas with parameters given in Table 2[15]. It must be remembered, however, that these are average values which will vary with look direction by 2-3×.
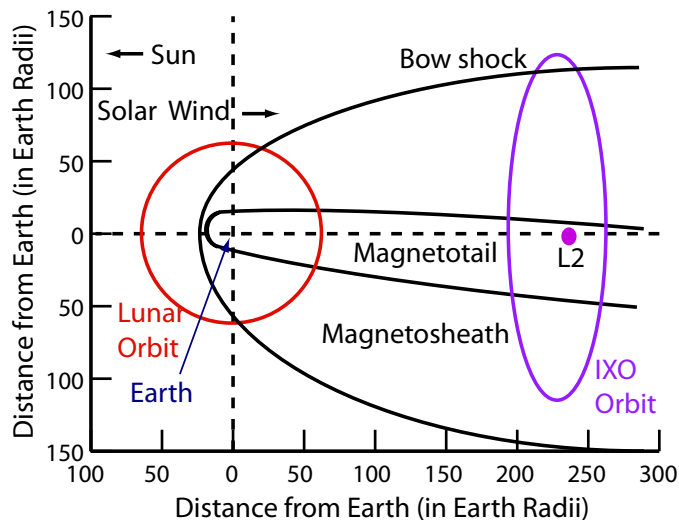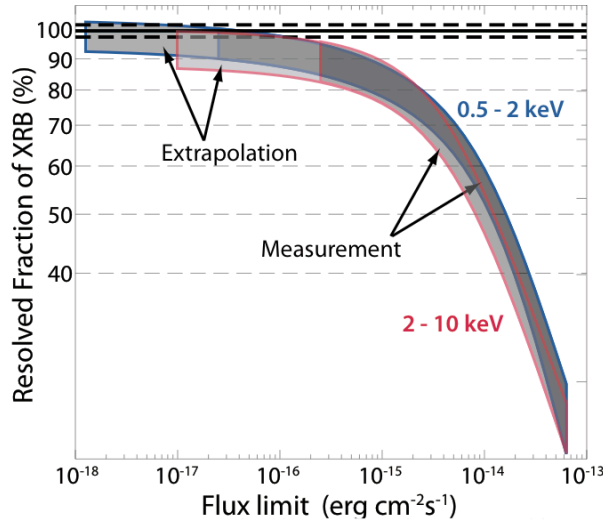
Figure 2 – Fraction of X-ray background between 0.5-2 (outlined in blue) and 2-10 keV (outlined in red) as a function of flux limit[18]; gray areas show the 1σ error region

2.3 Extragalactic Emission

Since both the local and Galactic components contribute a background dominated by emission lines, their effect depends entirely on the specific science under consideration and whether the source and background emission lines will be blended. However, the extragalactic background is predominantly a continuum source. Although controversies exist about the details, it is generally agreed that at high energies (E>2 keV), the CXB is due primarily to unresolved AGN. A recent measurement of the 2-8 keV background using XMM-Newton by de Luca & Molendi[17] used a single power law with photon index 1.41 and normalization 11.6 ph/cm^2/s/keV/sr.

However, this calculation does not consider the variation created by the point source origin of the extragalactic CXB. Over the entire sky, the number of sources brighter than a given flux [N(>S)] has been estimated by a number of groups. Figure 2, based on Moretti et al.[18], shows the fraction of the X-ray background in the 0.5-2 keV and 2-10 keV bands as a function of AGN flux. Table 1 lists the parameters for the number of sources brighter than a given flux (in the 1-2 keV and 2-10 keV bands) using the equation

$$N(>S) = N \times [(2 \times 10^{-15})^{\alpha 1}/(S^{\alpha 1} + S_0^{\alpha 1 - \alpha 2} S^{\alpha 2})] \text{ erg/cm}^2/\text{s/arcmin}^2. \quad (1)$$

Using these values, we see that the chance of finding a source with a $F_X > 3 \times 10^{-15}$, 10^{-14}, or 3×10^{-14} erg/cm^2/s in a given sq. arcmin is 10%, 3.5%, and 0.9% in the soft band, and 30%, 8.4%, and 1.9% in the hard band. As a result, although as noted above the average extragalactic background is ~0.006 cts/s/arcmin^2 between 2-10 keV for any detector/mirror combination, there is about a 1 in 30 chance that any given sq. arcmin region will actually have a 10^{-14} erg/cm^2/s source and so therefore a rate ~50× higher (~ 0.3 cts/s). Such a source will be easily detectable in a 1 ksec observation, and so is not truly part of the true diffuse background. Even short 10 ksec observations would detect ~300 counts from a 10^{-15} erg cm^{-2}s^{-1} source, so at least ~70% of the AGN background will be regularly resolved.

Table 1 CXB Parameters[18]		
	1-2 keV	2-10 keV
$\alpha 1$	1.82	1.57
$\alpha 2$	0.60	0.44
S_0	1.48 x 10^{-14}	4.5 x 10^{-15}
N	1.708	1.472

These results are not necessarily suitable for the HXI, however, as it has a much harder bandpass. Although based on older data, the all-sky HEAO-1 background covers a wider bandpass (3-40 keV) and was fit by Boldt[19] with the function

$$CXB(E_{keV}) = 9 \times 10^{-9}(E/3)^{-0.29}\exp(-E/40) \text{ erg/cm}^2/\text{s/sr/keV} = 6.5 \times 10^{-7} E^{-1.29}\exp(-E/40) \text{ ph/cm}^2/\text{s/keV/arcmin}^2 \quad (2)$$

Using the IXO response noted in the Appendix, in the 10-40 keV band, the HXI rate is 2.9×10^{-5} cts/s/arcmin^2 with the SPO mirrors. For the SPO mirrors, the de Luca & Molendi[17] value is 80% larger, so we use the Boldt[19] model for this instrument.

3. THE NON-X-RAY BACKGROUND

Unfortunately, there have been no X-ray missions to date at L2 (though WMAP and Herschel are there now, and JWST will be), so we have no direct information about how the particle background there will affect an X-ray detector. Therefore, we must use a combination of known information about the particle environment at L2, along with proxy measurements from other missions. There are a number of approaches available:

1. Use the known backgrounds from existing instruments. In the case of the XMS, we must use the value from

Figure 3 – Suzaku XRS non-X-ray background before gate value opening, with simple two-level fit (from [20]).

Figure 4 – Non-X-ray background spectra from: ASCA/SIS (green), Suzaku/XIS-FI (black), Suzaku/XIS-BI (red), XMM-Newton/PN (light blue), XMM-Newton/MOS(blue). Each spectra is normalized by the CCD area. (From [24])

the Suzaku XRS and then scale this by the ratio of the background seen with the XMM-Newton or Chandra CCDs to the Suzaku CCDs. This approach is simple, but suffers because the IXO L2 orbit is quite different from that of the XMM-Newton or Chandra orbit (elliptical, with a perigee about 1/3 of the lunar orbit; see Figure 1).

2. Estimate the number of energetic particles (primarily Galactic Cosmic Rays, or GCR) at L2 in the IXO orbit, and then predict the effect of these particles on the XMS, WFI, and HXI via either a comparison to existing satellites, or using a model of the spacecraft (e.g., a GEANT simulation).

As mission development proceeds we expect to use the second approach, but we use the simple scaling method here.

3.1 Recent X-ray Missions and their Backgrounds

Suzaku XRS: Kelley et al.[20] describe the performance of the Astro-E2 XRS in flight; their results are summarized here. Although no astronomical observations were completed, the XRS particle background was measured while the XRS was operational (See Figure 2). A number of models can be fit to this data; one simple approach is to simply fit a step function such that the background is

$$Bgd(E) \sim 6\times10^{-5} \text{ cts/s/keV/mm}^2 \quad (E<6 \text{ keV}) \quad (3)$$
$$Bgd(E) \sim 2.5\times10^{-5} \text{ cts/s/keV/mm}^2 \quad (E>6 \text{ keV}).$$

Figure 2 shows an analysis of 37.1 ksec of data taken between SAA crossings. The total rate in the anticoincidence detector during this period was 0.9 cts/cm^2/s. If this were generated by minimum ionizing particles, the calorimeter background rate would be 9×10^{-4} cts/cm^2/s given the known veto efficiency. However, the actual total rate of unvetoed events is 0.05±0.003 cts/cm^2/s, strongly suggesting that secondary particles dominate the background. For comparison, the GCR flux at L2[21] varies between 1.7-4.7 protons/cm^2/s, depending upon position in the Solar cycle (see Section 3.2).

Suzaku XIS: Yamaguchi et al.[22] modeled the XIS particle background with two components. The first component, contributing 80% of the background, consisted of protons and electrons of extraterrestrial origin, while the second component (contributing 20% of the background) was from electrons and protons produced by interactions of primary cosmic rays in the Earth's atmosphere. However, to reach agreement with the observed XIS background rate, the expected incident particle flux had to be multiplied by 3, for reasons not yet un-
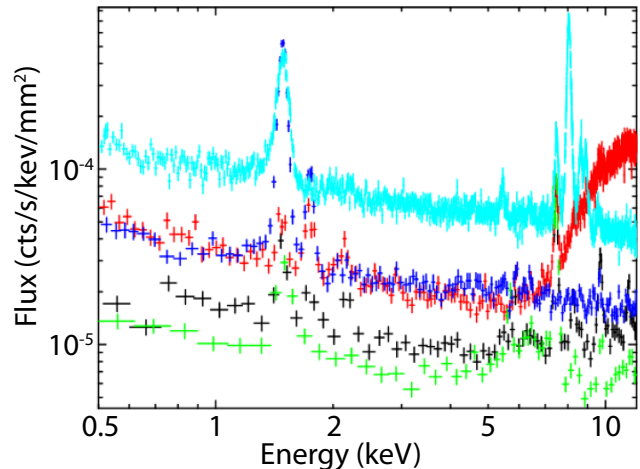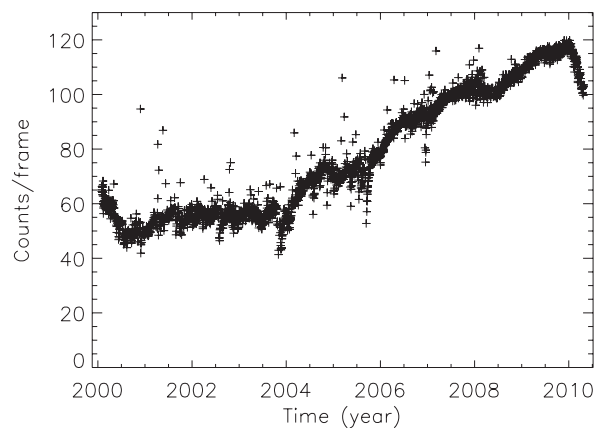

Figure 5 – Chandra high-energy (12-15 keV) count rate for the ACIS-S3 CCD as a function of year. Solar minimum was predicted for 2008, but actually arrived in late 2009 where the count rate peaked. (C. Grant, 2010)
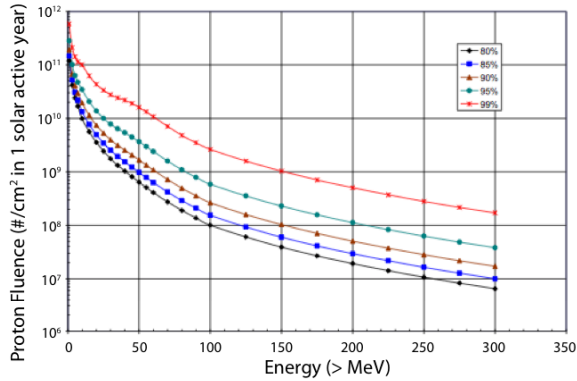
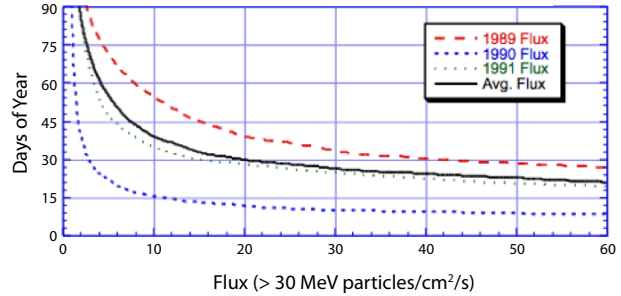Figure 6 – Solar proton fluences for 1 solar active year.

Figure 7 – Distribution in terms of number of days per year with solar proton flux counts with energies greater than 30 MeV.

derstood. There should be some modulation of the Galactic cosmic ray rate due to solar activity, but this has not yet been taken into account by the Suzaku team.

XMM-Newton: Hall & Holland[23] completed a detailed study, including GEANT simulations, of the XMM-Newton MOS detectors compared to the Swift CCDs of the same manufacture, as well as the Suzaku XIS CCD detectors. Their results found an increase of 3-4× in background due to XMM-Newton's large and highly elliptical orbit compared to Swift's low Earth orbit (LEO). Using GEANT simulations, this increase is consistent with the measured difference in GCR from 2.2 protons/cm^2/s in XMM-Newton's orbit (at Solar maximum; 2× larger at Solar minimum) to 0.6 photons/cm^2/s for Swift. Figure 4 shows a comparison of the Suzaku XIS and XMM-Newton EPIC rates, after dividing by the geometric area of the detectors in mm^2, taken from an internal Suzaku background report[24]. Although not identical like the Swift and XMM-Newton MOS CCDs, the primary differences between the XIS FI and EPIC MOS, and the XIS BI and EPIC PN detectors is that Suzaku is in LEO while XMM-Newton's orbit is much higher and well beyond the Earth's magnetosphere. As Figure 4 shows, the LEO reduces the overall background level by a factor of ~4.

Chandra: Like XMM-Newton, Chandra is in a large and highly elliptical orbit. Complicating the simple picture of a 3-4× increase in background, however, the measured raw particle rate in the HRC anti-coincidence detector was ~3 protons/cm^2/s, compared to an expected GCR flux of 4-5 protons/cm^2/s for Chandra's orbit. This suggested that there was some residual magnetic shielding in the Chandra orbit. Figure 5 (from C. Grant, http://space.mit.edu/home/cgrant/cti/cti120/bkg.ps) shows the Chandra background rate as a function of time. As expected, it is anti-correlated with solar activity, as is the GCR flux. This implies that the Chandra background is dominated by the GCR rate, with other components of lesser importance.

3.2 The Known Energetic Particles at L2

The particle background at L2 will be comprised of the standard components: Galactic Cosmic Rays and Solar Wind particles. Using the CREME96 (https://creme96.nrl.navy.mil) code for a satellite at L2. Sanwal[21] found a total flux of between 1.7 – 4.7 protons/cm^2/s at solar max and min, respectively. These values are quite similar to the values found by XMM-Newton and Chandra in their high Earth orbits, suggesting that the particle environment at L2 is similar to that found in high Earth orbits beyond the Earth's magnetosphere. This has been confirmed by data from the ESA standard radiation monitors which are on both near-Earth satellites (Rosetta, INTEGRAL) and, since late 2009, on those at L2 (Herschel, Planck). These monitors show a maximum increase of 4% in the high energy particle rate at L2 compared to high Earth orbits during solar minimum; at solar maximum these rates should go down[25].

The reduction at solar maximum is due to the fact that at maximum, the heliosphere expands and deflects a larger number of external particles. It should be noted, however, the Chandra and XMM-Newton experiences have showed that while the overall background increased at solar minimum, strong solar events that created flares were much more likely at solar maximum. Therefore both the steady (primarily GCR) and impulsive background (primarily solar) must be tracked, since they trade off each other.

Fortunately, the SOHO instrument is at L1 and has been measuring solar effects since 1995; in addition, data are available from the GEOTAIL satellite. In general the solar wind average 1-10 particles/cm^3, with a velocity of 400 km/s and a thermal energy of only a few eV. However, at times the thermal energy can increase to keV (although the density is then only ~0.1 particles/cm^3). There are also high-energy particles emitted by the Sun; the JWST mission has done a calcula-

Table 2 Summary of CXB and NXB rates							
		Silicon Pore Optics			Slumped Glass Optics		
	Model	**XMS**	**WFI**	**HXI**	**XMS**	**WFI**	**HXI**
CXB	*Normalization*	*cts/s/arcmin²* *(0.3-10 keV)*	*cts/s/arcmin²* *(0.1-15 keV)*	*cts/s/arcmin²* *(10-40 keV)*	*cts/s/arcmin²* *(0.3-10 keV)*	*cts/s/arcmin²* *(0.1-15 keV)*	*cts/s/arcmin²* *(10-40 keV)*
SWCX (2 LU)	0.002@0.57 [a]	0.17×10^{-2}	0.28×10^{-2}	0	0.19×10^{-2}	0.30×10^{-2}	0
LHB ($10^{6.14}$K)	4.5×10^{-3} [b]	0.63×10^{-2}	2.0×10^{-2}	0	0.73×10^{-2}	2.3×10^{-2}	0
Galactic ($10^{6.05}$K)	4.1×10^{-3} [b]	0.28×10^{-2}	0.89×10^{-2}	0	0.33×10^{-2}	1.0×10^{-2}	0
Galactic ($10^{6.46}$K)	1.7×10^{-3} [b]	0.63×10^{-2}	1.1×10^{-2}	0	0.71×10^{-2}	1.2×10^{-2}	0
AGN (Γ=1.41)	0.01@1 [d]	3.4×10^{-2}	4.9×10^{-2}	2.9×10^{-5}	3.6×10^{-2}	5.2×10^{-2}	n/a
NXB		*cts/s/keV/arcmin²*	*cts/s/keV/arcmin²*	*cts/s/keV/arcmin²*	*cts/s/keV/arcmin²*	*cts/s/keV/arcmin²*	*cts/s/keV/arcmin²*
Particle		8.1×10^{-3} [c]	1.7×10^{-3}	1.7×10^{-4}	8.1×10^{-3} [c]	1.7×10^{-3}	1.7×10^{-4}

[a] Units of ph/m²/s/arcmin² @ energy (keV)
[b] Units of cm⁻⁶pc; note the Galactic components are absorbed with N_H=1.3×10²⁰ cm⁻².
[c] Below 6 keV; above 6 keV, 3.4×10^{-3}
[d] Units of ph/m²/s/keV/arcmin² @ energy (keV); also absorbed with N_H=1.3×10²⁰ cm⁻².

tion of the flux of these particles[26] (see Figure 6). Note that these fluxes are for an entire year, although the report notes that the solar events that generate these particles are episodic, not continuous, and thus not linear in time. As a result, it is difficult to estimate what effect this will have on individual observations; obviously, during times of high incident solar particle flux no data will be used, and the satellite might even be put in safe mode.

Another view of the problem is shown in Figure 7, also from the JWST report[26], which shows how many days per year have particle fluxes above 30 MeV. The data show that, on average, there will be ~30 days in a given year with a flux of >30 MeV particles that is larger than 20 particles/cm²/s, and ~60 days where the rate of solar wind particles is similar to that of the GCR (i.e., ~4 protons/cm²/s). Note that a 30 MeV proton will stop in only 4 mm of Al, while a 100 MeV proton requires ~3 cm of Al to stop. Of course, GCR energies range from 1–10⁴ MeV, so a better comparison would need to include possible shielding and integration over the relevant particle distributions.

3.3   Scaling Results for IXO

The dominant source of non-X-ray background counts is expected to be GCR, except during the (aperiodic and excluded here) solar flares that will dominate the total dose. However, as noted above the actual GCR rate as a function of time and position in the solar system is not well known, although it does vary (inversely) with the solar cycle. The shielding provided by the Earth's magnetic field as a function of altitude is known to an extent; from the XMM-Newton to Suzaku comparison, we see that a factor of 4 increase is plausible. However, it should be noted that the Chandra background is lower than that of XMM-Newton, despite a similar orbit, so the situation is possibly more complicated. In addition, secondary particles and photons induced by GCR may be the most significant impact, generating a response in the IXO detectors similar to what occurred in the EPIC, ACIS, or XRS detectors. These could be modeled via a GEANT simulation, although it should be noted that such a simulation done pre-launch for the XRS significantly underestimated the true background[27], for reasons that are not entirely understood.

The Suzaku XIS background does correlate well with the Earth's magnetic field coefficient of rigidity (COR), suggesting the ionizing particles are coming from cosmic rays. Using the Webber-Lezniak[28] solar minimum cosmic ray spectrum convolved with the changes in the cut-off energy implied by the available range of COR values seen by Suzaku suggests that there should be a factor of 5 change as the COR changes from 14 to 4. However, the XRS anti-coincidence rate shows only a factor of 3 modulation; the XIS results show only a factor of 2 (see Figures 6, 7 of Katayama et al[24]). Therefore, there must be some component of the background that has a contribution similar to that from the GCR.

Considering these complications, we therefore use a simple model where the IXO NXB (per unit area) for the XMS is assumed to be four times that seen in the Suzaku XRS. Below 6 keV, this is ~ 2.4×10⁻⁴ cts/s/keV/mm², or in sky units assuming a 20m focal length mirror, 8.1×10⁻³ cts/s/keV/arcmin². Above 6 keV, the rate falls to ~ 10⁻⁴ cts/s/keV/mm² or 3.4×10⁻³ cts/s/keV/arcmin². This model is consistent with the IXO XMS requirement on the NXB background.

The WFI is an active pixel device, not a CCD, but our best model for the in-flight background is from the Suzaku, Chandra and XMM-Newton CCDs. Figure 4 shows a range from 10⁻⁵ - 2×10⁻⁴ cts/s/keV/mm² for the continuum back-

ground, ignoring fluorescence peaks. Picking a median value, we use 5×10^{-5} cts/s/keV/mm^2 as a typical value. In sky units using a 20m focal length, this is equivalent to 1.7×10^{-3} cts/s/keV/arcmin^2.

Suppressing the non-X-ray background in the HXI is a complex topic beyond the scope of this document. We therefore simply rely on the design specification that the NXB will be 5×10^{-6} cts/mm^2/s/keV $= 1.7 \times 10^{-4}$ cts/s/keV/arcmin^2 and largely energy-independent.

4.   OTHER EFFECTS

The CXB and NXB terms discussed above are inherent to any telescope, as the former are 'real' photons while at least some GCR will penetrate any amount of shielding. However, there are other background components whose strength is entirely a function of the telescope design. We mention these for completeness, but do not attempt to estimate their contribution as the IXO does not yet have a final approved design.
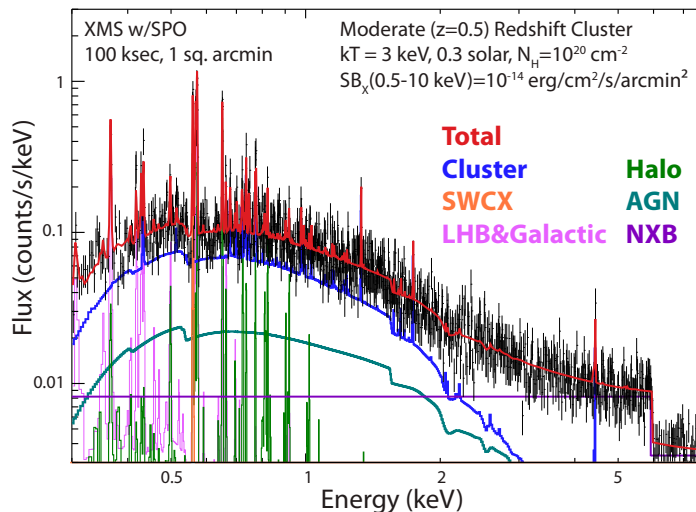

Figure 8 – Redshift 0.5 cluster observed with the IXO XMS assuming the silicon pore optics mirror. The red line shows the source plus background model, while the blue line shows the cluster by itself. The NXB is shown in purple, the AGN in teal, the SWCX in orange, the LHB and Galactic emission in pink, while the harder halo emission is in green.

4.1   Stray Light

In a standard two-reflection X-ray mirror design, stray light can occur when a zero- or single-bounce path through the mirror can reach a detector. Such photons usually arise from bright off-axis sources, and lead to 'arcs' fairly far from the aimpoint of the detector. This problem can generally be avoided by adding baffles to the telescope. In XMM-Newton, for example, the typical contribution is ~0.1% for a source 0.5-1.5 degrees off-axis. This problem can be significant when attempting to measure the CXB itself, though; in XMM-Newton the effect increases the observed diffuse background by ~7%. For IXO, we expect to implement baffles that will minimize stray light.

4.2   Optical Transmission from Bright Sources

X-ray detectors are generally also sensitive to IR, optical, and UV photons, which must be eliminated using filters. These filters, however, will have some transmission in non-X-ray bandpasses and so sufficiently bright sources – such as solar system objects like Jupiter or nearby stars such as Vega – will have some impact on the detectors. The actual effect is detector-dependent; Chandra's CCDs, for example, optical photons from bright sources induce a small additional charge in the pixels which leads to an offset in the detector bias of a few channels[29]. In the XMS microcalorimeter, optical photons will increase the baseline temperature slightly, adding noise to the system and decreasing the detector's sensitivity and resolution.

5.   SAMPLE IXO SOURCES INCLUDING BACKGROUND

Table 2 summarizes our results, showing expected surface brightnesses and expected count rates for the different CXB and the NXB terms. Figure 8 shows a sample source, a 100 ksec observation of a 1 sq. arcmin region selected out of a cluster at z=0.5 with kT = 3 keV and absorbed by $N_H = 10^{20}$ cm^{-2}. The cluster surface brightness was assumed to be SB_X(0.5-10 keV) = 10^{-14} erg/cm^2/s/arcmin^2. In this case, the non-X-ray background only begins to be a limiting factor above 2 keV. Although the cosmic X-ray background is significant below 1 keV, the redshifting of the lines in source cluster will enable their use in astrophysical analyses. Even in this lower bandpass, a number of strong lines can be easily identified, and would still be visible even at a 3-5 times lower flux level. More work remains to be done to determine where the true background limit would be for different cosmic sources (*e.g.* pointlike, diffuse) seen with IXO's various detectors.

6. REFERENCES

[1] Bookbinder, J. et al. 2010, arXiv:1001.2329v1

[2] Cox, D. P. & Reynolds, R. 1987, ARA&A, 25, 303

[3] Lallement, R. 2004, A&A, 418, 143

[4] Collier, M. et al. 2005, AdSpR, 35, 2157

[5] Koutroumpa, D. et al. 2006, A&A 460, 289

[6] Kuntz, K. D. & Snowden, S. L. 2008, A&A, 478, 575

[7] Snowden, S. L., Kuntz, K. D. & Collier, M. 2004, ApJ, 610, 1182

[8] Robertson, I. P., & Cravens, T. E. 2003, Geophysical Research Letters, 30, 080000

[9] Henley, D. B. & Shelton, R. L. 2010, ApJS, 187, 388

[10] Carter, J. A. & Sembay, S. 2008, A&A, 489, 837

[11] Henley, D. B. & Shelton, R. L. 2008, ApJ, 676, 335

[12] Snowden, S. L. et al. 1990, ApJ, 354, 211

[13] Sanders, W. T. et al. 2001, ApJ, 554, 694

[14] Smith, R. K. et al. 2007, PASJ, 59S, 141

[15] Kuntz, K. 2010, private communication based on Table 2 of [6].

[16] Kuntz, K. D. & Snowden, S. L. 2000, ApJ, 543, 195

[17] De Luca, A. & Molendi, S. 2004, A&A, 419, 837

[18] Moretti, A. et al. 2003, ApJ, 588, 696

[19] Boldt, E. 1987, Physics Reports, 146, 215

[20] Kelley, R.et al. 2007, PASJ, 59S, 77

[21] Sanwal, D. 2005, Con-X Observing Efficiency internal report (05-Nov-08)

[22] Yamaguchi, H. et al. 2006, SPIE, 6266E, 121

[23] Hall, D. & Holland, A. 2009, Nucl Inst. & Methods A, 612, 320

[24] Katayama, H. et al. 2005, "Suzaku/XIS background report", http://www-cr.scphys.kyoto-u.ac.jp/member/matumoto/XIS/background/xis_background_20051216.pdf

[25] Lumb, D. 2010, private communication

[26] Barth, J. L., Isaacs J. C. & Poivey, C. 2000, "The Radiation Environment for the Next Generation Space Telescope", http://ridl.cis.rit.edu/products/IDTL%20products/publications/ngstradenv2.pdf

[27] Saab, T. et al. 2004, SPIE, 5501, 320

[28] Webber, W. R. & Lezniak, J. A. 1974, Ap&SS, 30, 361

[29] Chandra Proposer's Guide, Section 6.3, http://cxc.harvard.edu/proposer/POG/html/chap6.html

APPENDIX

We show in Table 3 the full names of the response matrices used in this work; these files are available on the IXO webpage at http://ixo.gsfc.nasa.gov.

Table 3 Response Matrices Used		
Detector	**Glass**	**Silicon Pore**
XMS	ixo_glass_xms_inner_0p5_20100704.rsp	ixo_xms_none_20100527.rsp
WFI	ixo_glass_wfi_open_20100704.rsp	ixo_wfi_open_20100527.rsp
HXI	n/a	ixo_hxi_none_20100527.rsp